HYDROPHOBICALLY MODIFIED AMPHIPHILIC BLOCK COPOLYMER MICELLES IN NON-AQUEOUS POLAR SOLVENTS. FLUOROMETRIC, LIGHT SCATTERING AND COMPUTER-BASED MONTE CARLO STUDY+

Pavel MATĚJÍČEK[a1], Filip UHLÍK[a2], Zuzana LIMPOUCHOVÁ[a3], Karel PROCHÁZKA[a4,*], Zdeněk TUZAR[b] and Stephen E. WEBBER[c]

[a] *Department of Physical and Macromolecular Chemistry and Laboratory of Specialty Polymers, Charles University, Albertov 6, 128 43 Prague 2, Czech Republic; e-mail: [1] matej@merlin.natur.cuni.cz, [2] uhlik@natur.cuni.cz, [3] zl@vivien.natur.cuni.cz, [4] prochaz@vivien.natur.cuni.cz*

[b] *Institute of Macromolecular Chemistry, Academy of Sciences of the Czech Republic, Heyrovského nám. 2, 162 06 Prague 6, Czech Republic; e-mail: tuzar@imc.cas.cz*

[c] *Department of Chemistry and Biochemistry, University of Texas at Austin, Austin, TX 787 12, U.S.A.; e-mail: cmsew@mail.utexas.edu*

Received December 21, 2001
Accepted March 8, 2002

The micellization behavior of a hydrophobically modified polystyrene-*block*-poly(methacrylic acid) diblock copolymer, PS-N-PMA-A, tagged with naphthalene between blocks and with anthracene at the end of the PMA block, was studied in 1,4-dioxane–methanol mixtures by light scattering and fluorescence techniques. The behavior of a single-tagged sample, PS-N-PMA, and low-molar-mass analogues was studied for comparison. Methanol-rich mixtures with 1,4-dioxane are strong selective precipitants for PS. Multimolecular micelles with compact PS cores and PMA shells may be prepared indirectly by dialysis from 1,4-dioxane-rich mixtures, or by a slow titration of copolymer solutions in 1,4-dioxane-rich solvents with methanol under vigorous stirring. In tagged micelles, the naphthalene tag is trapped in nonpolar and fairly viscous core/shell interfacial region. In hydrophobically modified PS-N-PMA-A micelles, the hydrophobic anthracene at the ends of PMA blocks tends to avoid the bulk polar solvent and buries in the shell. The distribution of anthracene tags in the shell is a result of the enthalpy-to-entropy interplay. The measurements of direct nonradiative excitation energy transfer were performed to estimate the distribution of anthracene-tagged PMA ends in the shell. The experimental fluorometric data show that anthracene tags penetrate into the inner shell in methanol-rich solvents. Monte Carlo simulations were performed on model systems to get reference data for analysis of time-resolved fluorescence decay curves. A comparison of experimental and simulated decays indicates that hydrophobic traps return significantly deep into the shell (although not as deep as in

+ The study is a part of the long-term Research Plan of the School of Science No. MSM 113100001.

aqueous media). The combined light scattering, fluorometric and computer simulation study shows that the conformational behavior of shell-forming PMA blocks in non-aqueous media is less affected by the presence of nonpolar traps than that in aqueous media.
Keywords: Micelles; Block copolymers; Micellization; Fluorometry; Monte-Carlo simulations; Conformational behavior.

Steady-state and time-resolved fluorometry have proved to be very useful tools for studying synthetic polymers and biologically important macromolecules[1,2]. Nonradiative excitation energy transfer (NRET) ranks among common fluorescence techniques. It has been used in studies of polymer compatibility and conformational changes[3–8]. Several authors applied NRET also to investigation of polymeric micelles[9–13].

Polymeric micelles form spontaneously upon dissolution of a block copolymer AB in a selective solvent (solvent for block A and simultaneously a nonsolvent for block B)[14]. In most cases, they are spherical and contain a compact insoluble core (formed by blocks B) and a protective shell (formed by blocks A). They consist of several tens to few hundreds of associated chains (depending on the solvent selectivity) and their hydrodynamic radius ranges from 30 to 60 nm. Hydrophobic/hydrophilic block polyelectrolytes form reversible micelles in polar solvents and in aqueous mixtures with excess organic solvents[15]. They may form also micelle-like nanoparticles with ionized polyelectrolyte blocks in aqueous media[16–26]. However, block polyelectrolyte samples with long hydrophobic blocks are usually insoluble in water and micelles have to be prepared indirectly, *e.g.*, by dialysis[27,28]. The cores of high-molar-mass polyelectrolyte micelles are usually kinetically frozen in water (*e.g.*, the polystyrene cores are in glassy state) and the micellar properties are controlled by the polyelectrolyte behavior of the shell[28].

Some amphiphilic block copolymers form kinetically frozen micellar systems also in very strong selective organic solvents, *e.g.*, polystyrene-*block*-poly(methacrylic acid) diblock copolymer in methanol-rich mixtures with 1,4-dioxane[27]. In such a case, micelles may be prepared either by dialysis or by a slow titration. Polystyrene cores are compact and basically behave as those in water. Since the dissociation of poly(methacrylic acid) is negligible in methanol-rich organic media, the shell-forming blocks behave differently compared with aqueous solutions. We have been studying the micellization of high-molar-mass block copolymers and polyelectrolytes in polar and aqueous media systematically for a long time, both experimentally and theoretically[27–37]. In this paper, we study behavior of hydro-

phobically modified micelles of polystyrene-*block*-poly(methacrylic acid) in 1,4-dioxane–methanol mixtures by light scattering and fluorometry. We also present a model for interpretation of NRET data in solutions of polymeric micelles with fluorophores attached to specific parts of copolymer chains.

EXPERIMENTAL

Material

Block copolymer samples. Polystyrene-*block*-poly(methacrylic acid), (i) a single-tagged sample, PS-N-PMA, with one pendant naphthalene tag between blocks and (ii) a double-tagged sample, PS-N-PMA-A, with one pendant naphthalene tag between blocks and one anthracene tag at the end of the poly(methacrylic acid) block, were prepared at the University of Texas at Austin using anionic polymerization in tetrahydrofurane at –78 °C in N_2 atmosphere, as described earlier[27,28]. The PS block was prepared first, then a small amount of 2-vinylnaphthalene (*ca* one tag per chain) was added followed by a high excess of *tert*-butyl methacrylate. Adding a very low percentage of the fluorescent comonomer with convenient values of copolymerization parameters results in a narrow distribution of naphthalene tags in different chains. Termination of the polymerization was achieved by adding either a solution of CH_3OH in the case of PS-N-PMA or 9-(chloromethyl)anthracene in the case of PS-N-PMA-A, which leads theoretically to a quantitative tagging of each copolymer chain by one terminal 9-anthryl group. The average content of fluorophores was checked by UV-VIS absorption measurements using the molar absorption coefficients of 2-methylnaphthalene and 9-methylanthracene. It was found close to 1.0 naphthalene tag per PS-N-PMA chain and 1.0 naphthalene and 1.0 anthracene tag per PS-N-PMA-A chain. The average copolymer composition was determined by NMR before hydrolysis. The molar mass and polydispersity of the first block and of the diblock were measured by size-exclusion chromatography and by static light scattering before hydrolysis. The pertinent experimental values are given in Table I. The sample was then hydrolyzed by heating with an excess of 6 M aqueous HCl in tetrahydrofuran at 85 °C for 5 h (2 mol of HCl per 1 mol of PMA to be formed). The dried sample was redissolved in 1,4-dioxane and freeze-dried. The degree of hydrolysis was estimated by NMR and was found close to 1.00 (0.98–0.99). The structure of both copolymer samples is schematically shown in Chart 1.

Preparation of polymeric micelles in mixed solutions. Solutions of fluorescently tagged PS-PMA micelles were prepared by direct dissolution of the copolymer in 1,4-dioxane and by slow titration by methanol (under vigorous stirring) up to the desired solvent composition.

Techniques

Static light scattering (SLS). Measurements were performed on a Sofica instrument equipped with a He-Ne laser. Data were treated by the standard Zimm method. Refractive index increments, dn/dc, were measured on a Brice–Phoenix differential refractometer. When mixed solvents were employed, effective values of $(dn/dc)_\mu$ were measured under the condition of osmotic equilibrium between the solution and the mixed solvent, using a fixed volume dialysis cell[38].

TABLE I
Characterization of polymers and micelles determined by SLS (in a mixture 1,4-dioxane–methanol (80 vol.%))

Sample	M_w, kg mol^{-1}	x_{PS}[a]	M_w/M_n (P_D)[b]
Polymers			
PS-N-PMA-A	60.6	0.52	1.09
PS-N-PMA	54.4	0.42	1.15
Micelles			
PS-N-PMA-A	$10.6 \cdot 10^3$	0.52	<0.1
PS-N-PMA	$9.5 \cdot 10^3$	0.42	<0.1

[a] Mass fraction of PS, x_{PS}, determined by NMR. [b] For micelles, P_D, determined from the second moment of the DLS autocorrelation curve, $g^{(1)}(t)$. For copolymers, M_w/M_n, determined by size exclusion chromatography.

PS-N-PMA-A

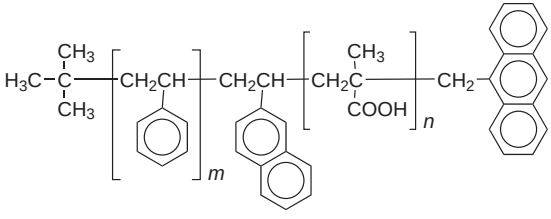

m = 300, n = 340

PS-N-PMA

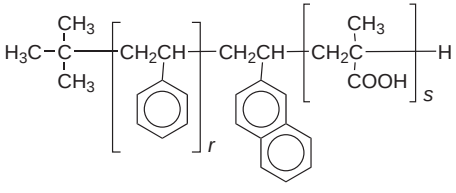

r = 220, s = 365

CHART 1
Structure of copolymers PS-N-PMA-A (a) and PS-N-PMA (b)

Dynamic lightsScattering (DLS). An ALV 5000 multibit, multitau autocorrelator (Langen, Germany) and a He-Ne laser (λ = 633 nm) were employed. Measurements were performed with solutions of the lowest concentration at an angle of observation 90° at 25 °C. Data were processed using a regularization algorithm REPES (ref.[39]) as described in detail previously[31,32]. Hydrodynamic radius R_H was evaluated from the diffusion coefficient using the Stokes–Einstein formula. The viscosity and refractive indexes of 1,4-dioxane–CH_3OH mixtures necessary for calculation of R_H values were estimated experimentally and are given in Table II. Polydispersities of micelles were evaluated from the second moment of the autocorrelation curve, $g_1(t)$.

Steady-state fluorometry. Steady-state fluorescence spectra (*i.e.*, corrected excitation and emission spectra and steady-state anisotropy) were recorded with a SPEX Fluorolog 3 fluorometer in 1-cm quartz cuvette closed with a Teflon stopper. Oxygen was removed by 5 min bubbling with nitrogen before the measurement.

Time-resolved fluorometry. The time-correlated single photon counting technique was used for measurements of fluorescence lifetimes. The time-resolved fluorescence decays were recorded on a ED 299 T time-resolved fluorometer, Edinburgh Instruments, Inc., equipped with a nanosecond coaxial discharge lamp filled with hydrogen at $5.01 \cdot 10^4$ Pa (pulse halfwidth *ca* 1.2 ns)[31,32]. The apparatus allows for a multiplexing regime of the simultaneous acquisition of fluorescence and excitation profiles (SAFE). A reconvolution procedure was used to get the true fluorescence decays that were further fitted to multiexponential functions using the Marquardt–Levenberg non-linear least squares method. Low values of χ^2 (close to 1.0) and random distribution of residuals were used as criteria of the fit.

MONTE CARLO SIMULATIONS

Monte Carlo simulations were performed on model systems to get reference pseudo-experimental data for comparison with measured fluorescence decays and energy transfer efficiencies and for evaluation of the average distance of energy traps from the core/shell interface.

TABLE II
Relative viscosity, η, and refractive index, n_D^{20}, of 1,4-dioxane–methanol mixtures

x_{MeOH}	η	n_D^{20}
0.45	0.618	1.379
0.55	0.583	1.370
0.60	0.567	1.366
0.75	0.533	1.351
0.80	0.525	1.346
0.90	0.513	1.336

Let us assume a system of N_T randomly distributed, fixed traps around a donor that was excited at $t = 0$. The survival probability, $\rho(t)$, that the donor is still excited at t is given by the following master equation[40]

$$\frac{d\rho}{dt} = -\left[\frac{1}{\tau_D} + \sum_{i=1}^{N_T} k_{tr}(r_i)\right]\rho , \qquad (1)$$

where τ_D is the effective fluorescence lifetime of the donor in a given medium (unaffected by NRET to traps) and $k_{tr}(r_i)$ are the transfer rate constants depending on the donor-to-trap distances, r_i. If the energy transfer occurs *via* the Förster dipole–dipole exchange mechanism, then $k_{tr}(r) = (1/\tau_D)(R_0/r)^6$, where R_0 is the Förster radius[41]. It is a distance for which $k_{tr}(R_0) = k_{eff} = 1/\tau_D$, k_{eff} being the effective fluorescence decay rate constant in the absence of traps. The solution of Eq. (*1*) yields the survival probability $\rho(t)$ for a given fixed configuration of traps with respect to the excited donor.

In a macroscopic system of fluorophores, the survival probability must be averaged over all donor-to-trap distances. Since the work of El-Sayed[42], Klafter and Blumen[43,44], Fayer and coworkers[45–48] and others, it has been recognized that energy transfer kinetics in infinite media depends only on the distribution of traps, while in restricted dimensions, the locus of donors (and also the finite number of traps) has to be taken into account. Following the Klafter–Blumen formalism[44], Winnik and coworkers derived formulae describing energy transfer in limited systems with spherical symmetry[49–51]. However, the micellar system studied here is different from that treated by Winnik *et al.*[51]. The traps are attached to the ends of the shell-forming blocks that are "tethered" to the core/shell interface. Individual traps are not equivalent with respect to the excited donor. One of the traps belongs to the same polymer chain as the excited donor, while the others do not. Any trap may come to the place separated by r from the excited donor. However, each of them will come there with a different probability. The Yekta–Winnik approach (using the function $4\pi r^2 C(R,r)$ which is proportional to the probability of finding a trap in the distance r from a donor that is positioned at R)[51] cannot be directly applied. We propose a new approach for analyzing fluorescence decays in double-tagged micellar systems. The analysis assumes a comparison of experimental decays with numerical Monte Carlo data. The model used reflects the structure of real micelles and is based on the following assumptions.

1) Micelles are monodisperse and spherical. They contain compact cores of the radius R_C. Since the energy donors are chemically attached to a bridge connecting the core-forming and the shell-forming blocks, we assume that, when micelles are formed, all donors are distributed homogeneously in fairly narrow spherical interfacial core/shell region, with a constant surface density.

2) The hydrophobic traps attached at the ends of the hydrophilic blocks try to avoid the polar medium. Since the hydrophilic polymer blocks are less polar than solvent molecules[27–30] and the concentration of their segments in the inner shell is high, the traps try to return into the shell, *i.e.*, towards the core and force the chains either to adopt fairly collapsed conformations or to recoil back towards to core and to form loops. Both the aforementioned conformations are entropically unfavorable. Therefore, the distribution of traps in the shell is the result of the enthalpy-to-entropy competition.

3) According to current experimental conditions used in fluorescence studies, only one (or more frequently none) donor per micelle is excited. Due to spherical symmetry of the system, all donors excited in different micelles are statistically equivalent. The micellar solution is very dilute. We consider NRET within one micelle only. When one donor is excited, different acceptors are neither independent nor statistically equivalent since one of them belongs to the same chain, while the others do not (see Scheme 1).

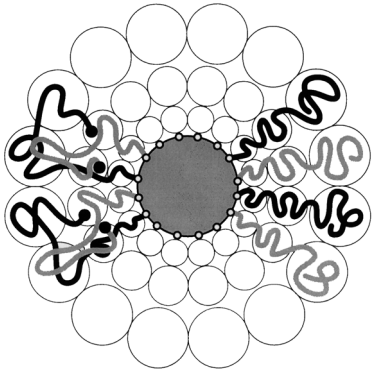

SCHEME 1

The proposed structure of (i) modified (left-hand side) and (ii) non-modified PS-PMA micelles in polar solvents (right-hand side) according to the blob-model that is believed to represent correctly the structure of a neutral *(i.e.,* non-charged) micellar shell in an organic solvent[14]. Neighboring PMA chains are in different colors to get a clear picture. Open circles indicate the blob size

In the computer study, we generate a high number $4 \cdot 10^5$ of individual sets of N_T traps in the shell using *a priori* probabilities $\varphi_i(\boldsymbol{r}_i)$ (which describe probabilities of finding individual traps in positions $\boldsymbol{r}_i$ in the shell – see below) and calculate fluorescence decays, $I_D(t)$, and transfer efficiency (the ratio of the rate of the excitation energy transfer for donors to traps to the rate of all processes that deplete the excited state of donors), χ_{tr}, for each configuration. Then we calculate the ensemble averages by computer-based Monte Carlo simulations using the generic averaging formulas

$$I_D^q(t) / I_0 = \left\langle \exp\left\{-\frac{t}{\tau_D}\right\} \prod_{i=1}^{N_T} \exp\left\{-\left[\frac{R_0}{r_i}\right]^6 \left[\frac{t}{\tau_D}\right]\right\} \right\rangle_M \qquad (2)$$

$$\chi_{tr} = \left\langle \frac{\dfrac{R_0^6}{\tau_D} \displaystyle\sum_{i=1}^{N_T} \frac{1}{r_i^6}}{\dfrac{R_0^6}{\tau_D} \displaystyle\sum_{i=1}^{N_T} \frac{1}{r_i^6} + \frac{1}{\tau_D}} \right\rangle_M , \qquad (3)$$

where I_0 is the fluorescence intensity at $t = 0$ and $\langle\rangle_M$ means the averaging over the macroscopic ensemble of micelles using an appropriate distribution function of donor-to-trap distances depending on the considered model.

Random Distribution of Traps in the Shell (3D-Random Model)

As it was already mentioned, the hydrophobic traps try to avoid the polar solvent and they bury themselves in the shell. The shell-forming blocks may either adopt partially collapsed conformations or recoil back and form loops. Both the chain collapse and the chain recoil are unfavorable from the entropy point of view and the distribution of traps in the shell is a result of the enthalpy-to-entropy interplay. As predicted by theoreticians, fairly broad distributions of chain sizes could be expected in modified polymer brushes under conditions similar to those in our systems[52]. Therefore, we study a system with a random distribution of traps first. The model of the fully relaxed shell represents a limit of the conformational behavior of the shell-forming blocks. It can actually be treated according to Winnik *et al.*[51], but it is very easy to perform the computer simulation and to get curves for the same structural parameters as those for more sophisticated

models. We assume that the random distribution of traps in the whole shell is only little probable in the studied system. Since fluorometry is an indirect experimental technique and the interpretation of time-resolved data for complex systems is model-dependent, the 3D-random model has to be considered and studied as well. Only a detailed comparison of simulated decay curves for several models makes it possible to discriminate between various distributions.

Random Angular Distribution of Traps Distributed in a Fixed Distance from the Core/Shell Interface (Degenerated 2D-Random Distribution Model)

In this model, we assume that all trap-modified ends of the shell-forming blocks are placed at the same distance, R_T, from the core/shell interface, but their positions fluctuate on the spherical surface. This model is a special limiting case of the previous 3D model, degenerated to the spherically curved 2D surface.

Maxwellian Model (M Model)

The third model assumes that the angular distribution of traps is a random one but the distribution in the radial direction passes a maximum. The *a priori* distribution function in the radial direction is expressed by the Maxwellian function, $\varphi(r) = A(r - R_C)^2 \exp[-(r - R_C)^2/(2\sigma^2)]$, where r is the distance from the micellar center, R_C is the core radius, and A and σ are constants (the former related to the normalization and the latter to the average distance of traps from the core). This particular function is used since it may be, in the first approximation, justified by "mean field-like" arguments[53–56] which we have recently shown in paper[57]. When using the Maxwellian distribution function, the normalization factor may be expressed as $A = 2/[\sqrt{(2\pi)}\sigma^3]$, the mean radial distance as $\langle r \rangle = R_C + 2\sigma\sqrt{(2/\pi)}$, the standard deviation is $\sigma(2 - 8/\pi)^{1/2}$ and the mode is $R_C + \sigma\sqrt{2}$.

Simplistic Reference System

To compare results of Monte Carlo simulations with a physically straightforward model and to analyze the influence of the non-randomness in the distribution of traps in the shell, we consider a very simple reference system. We assume that all traps are located at the same distance R_T from the core center and are uniformly "smeared" on that surface, with a surface density, $n_T = N_T/(4\pi R_T^2)$. For such a system of "uniform" micelles, we have

shown that the NRET-quenched donor fluorescence decays faster compared with that unaffected by NRET, but the decay is single-exponential[57]. The mean energy transfer rate constant and the transfer efficiency are given by the formulae, $(k_{mean}) = (R_0^6 N_T)(R_T^2 + R_C^2)\tau_D^{-1}(R_T^2 - R_C^2)^{-4}$ and $\chi_{tr} = (R_T^2 + R_C^2)/[R_T^2 + R_C^2 + (R_T^2 - R_C^2)^4/(R_0^6 N_T)]$. The derived analytical formulae allow for a simple calculation of the fluorescence decay curves and the NRET efficiency for the reference system.

RESULTS AND DISCUSSION

Characterization of Micellar Systems in 1,4-Dioxane–Methanol Solvents by SLS and DLS

Molar masses of micelles in a strong selective 1,4-dioxane–CH_3OH (80 vol.%) solvent were measured by static light scattering. They are given in Table I together with characteristics of unimers. The micellar molar masses are very similar for both types of micelles which is a reasonable result since both copolymer samples have quite similar molar masses and composition. We have recently observed an analogous association behavior of both samples in 1,4-dioxane–H_2O mixtures[58].

Basic characterization of micellar sizes was performed by DLS. Experimental data are presented in Fig. 1. They show the presence of only one kind of

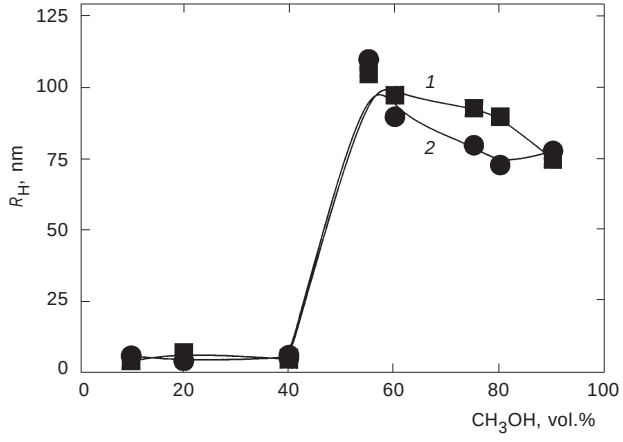

FIG. 1

Hydrodynamic radii, R_H, of polystyrene-*block*-poly(methacrylic micelles) formed by the double-tagged PS-N-PMA-A (*1*) and the single-tagged PS-N-PMA sample (*2*) in 1,4-dioxane–methanol mixtures. The curves are just guidelines for eyes

particle in all solutions, ascribed either to unimers (in mixtures containing less than 40 vol.% of CH_3OH) or to fairly monodisperse micelles (in methanol-rich mixtures). The polydispersity in micellar sizes, evaluated from the first cumulant of the autocorrelation curve, was always lower than 0.1. Curve *1* shows the hydrodynamic radius, R_H, of PS-N-PMA-A micelles and curve *2* that of PS-N-PMA, as functions of the solvent composition. In both cases the hydrodynamic radii, R_H, are very small in solvents with less than 40 vol.% CH_3OH since they correspond to unimers. Then they increase significantly with increasing content of methanol indicating the presence of multimolecular micelles. Hydrodynamic radii of the double-tagged and single-tagged micelles are almost the same (in corresponding solvents). In this respect, the behavior of double-tagged micelles differs from that in aqueous mixtures[58]. This behavior will be discussed in detail later together with NRET results.

Steady-State Fluorometric Measurements

In the fluorometric study, we have compared the behavior of two diblock copolymers: (i) the single-tagged, PS-N-PMA, and (ii) the double-tagged, PS-N-PMA-A, with similar molar masses and composition. The double tagging of the copolymer with naphthalene between PS and PMA blocks and with anthracene at the end of PMA block allows for the NRET study of the distribution of anthracene traps in the shell and the average distance of the ends of the modified shell-forming PMA block from the core/shell interface. Napthalene (energy donor, D) and anthracene (energy trap, T) represent a suitable pair of fluorophores which was often used in NRET measurements for the evaluation of end-to-end distances of polymer chains and other structure characteristics of various polymer systems. Holden and Guillet[7], Liu and Guillet[8], and Martin and Webber[59] proposed and tested several methods that yield correct estimates of distances between naphthalene and anthracene in different polymeric systems.

When fluorometric measurements are applied to polymeric micelles, optical conditions differ from common polymer systems and important corrections have to be done. In this paragraph, we briefly discuss the crucial ones. In the micellar systems studied, all naphthalene tags are localized in a narrow core/shell interfacial region. Due to the proximity of the PS shell, the micropolarity of the interface is low and the nondissociated PMA forms compact and fairly hydrophobic inner layer, not only in organic polar solvents but also in water at low pH (refs[32,33,58]). The high microviscosity affects the fluorescence quantum yield of naphthalene in comparison with

non-viscous solvents. In micellar systems, the polarity of the naphthalene microenvironment does not change with methanol content. The strongly hydrophobic anthracene tags attached to the ends of PMA blocks try to avoid the polar medium. As explained in previous parts, we expect that the anthracene tags are buried in the inner hydrophobic part of the shell fairly close to the naphthalene tags.

The emission intensity, $I_D^0(\lambda_D)$, of a naphthalene donor D (excited at wavelength λ_D in the absence of energy traps) is proportional to the intensity of the light, I_D^{abs}, absorbed by the donor D, and to its fluorescence quantum yield, ϕ_D^0, that takes into account all processes that, in a given medium without energy traps, compete with the emission at λ_D. The intensity, I_D^{abs}, is related to the proper value of the absorbance, $A_D(\lambda_D)$. However, the experimentally measured absorbance, $A_{exp}(\lambda_D)$, is due, in major part, to inactive absorption by the polymer backbone and to light scattering. Just a small part of the absorbed light (that may be expressed by $A_D(\lambda_D) = \varepsilon_D(\lambda_D)c_D l$, where $\varepsilon_D(\lambda_D)$ is the molar absorption coefficient of the donor, c_D its molar concentration, and l the optical path) is responsible for the excitation of donors. The inactive part makes almost 100% of the measured value and causes a strong attenuation of the excitation-active incident light. The corrected fluorescence intensity is given by the following expression

$$\left(I_D^0\right)_0 \cong \phi_D^0 I_0^{cor}(\lambda_D) 10^{-A_{exp}(\lambda_D)} S_D(\lambda_D) 2.3\varepsilon_D(\lambda_D) c_D l \,, \qquad (4)$$

where $I_0^{cor}(\lambda)$ is the wavelength-corrected lamp intensity and the correction factor $S_D(\lambda)$ describes changes in the fluorophore (donor) properties after its attachment to the polymer chain and a possible energy transfer from the backbone to the pendant fluorophore. This term reflects the most unpleasant complication in the data treatment and evaluation of the transfer efficiency. The pertinent correction has to be investigated and assessed experimentally using the studied copolymer and low-molar mass model compounds. In the case of NRET from a donor D to a trap T, the part $(1 - \chi_{tr})$ is emitted at λ_D, while the part, χ_{tr}, is transferred to T.

In order to interpret the steady-state results correctly, we have to recognize that while both samples are similar, they are not identical, and the same is true of the micelles formed from them. Micellar solutions strongly scatter the UV light and experimental absorbances of solutions used for fluorescence measurements are high, exceeding 1.0 in strong selective solvents. Therefore even small relative differences are important. The attenua-

tion of the incident light is not equal in both systems and the light absorbed by naphthalene in PS-N-PMA and PS-N-PMA-A micelles differs. If the measurements are performed for the same concentrations of single- and double-tagged micelles, the transfer efficiency, χ_{tr}, may be obtained from the following formula (some terms in Eq. (*4*) compensate, but not all of them)

$$\chi_{tr} = 1 - \frac{\left(I_D^q\right)_2}{\left(I_D^0\right)_1} 10^{-\Delta A_{exp}} \left(\frac{c_{D1}}{c_{D2}}\right), \qquad (5)$$

where $(I_D^0)_1$ and $(I_D^q)_2$ are fluorescence intensities from the single-tagged (1) and the double-tagged (2) micellar systems, respectively, $\Delta A_{exp} = (A_{exp2}) - (A_{exp1})$ and c_{D1} and c_{D2} are concentrations of donor tags per unit weight of the pertinent copolymer.

Figure 2 shows the excitation spectra of the anthracene tag (full curves *1* and *2*), the naphthalene tag (dashed curves *3* and *4*) in the double-tagged polymer, and PS-N-PMA-A in 1,4-dioxane–methanol mixtures with 5 and 90 vol.% methanol, respectively. The spectra show very pronounced solvent-dependent shifts. However, it is necessary to keep in mind that the

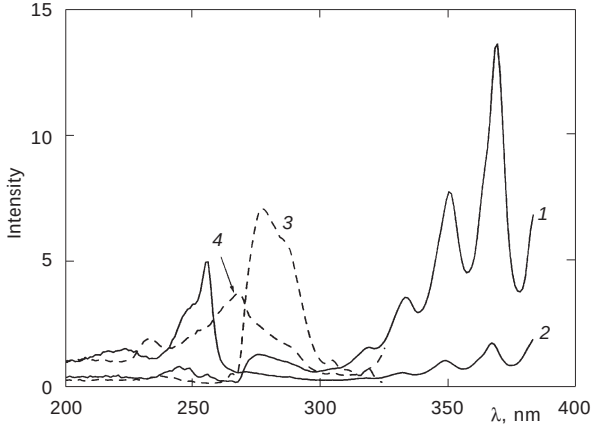

FIG. 2

The steady-state excitation spectra of fluorescent tags in solutions of polymeric samples: anthracene tag in the double-tagged PS-N-PMA-A in 1,4-dioxane with 5 and 90 vol.% CH_3OH (full curves *1* and *2*, respectively), naphthalene tag in the double-tagged PS-N-PMA-A sample in the same solvents (dashed curves *3* and *4*); mass concentration of polymers, $c = 1.5$ g l^{-1}, fluorescence intensities in arbitrary units (measured with constant widths of excitation and emission slits)

changes are due, in part, to energy transfer and also to changes in the rigidity of the microenvironment. When micelles are formed, the fluorophores are hidden in the shell. Naphthalene is embedded in the rigid core/shell interfacial region and this is why its fluorescence quantum yield increases (all fluorescence intensities from micelles in mixtures with 90 vol.% CH_3OH were reduced by a factor of 2 to get a clear picture). The naphthalene excitation spectra in micelles are shifted to lower wavelengths. Besides the above mentioned microenvironment rigidity, several other factors affect the spectral differences: (i) methanol is more transparent than 1,4-dioxane in this spectral region, (ii) scattering from micelles in methanol-rich solvent attenuates the incident light. The blue part of the excitation spectrum of the anthracene tag shows an apparent environment-dependent spectral shift. However, this shift (*i.e.*, a pronounced increase between 260 and 275 nm) is due to the energy transfer from naphthalene, since the micellar structure with anthracene traps buried in the shell allows for efficient NRET. The environment-dependent shift in naphthalene excitation maximum position (together with absolute intensity changes) indicates that the excitation wavelength has to be chosen properly and all corrections (mainly the contribution of the direct anthracene excitation and pertinent quantum yields) have to be evaluated for individual solutions independently and very carefully.

Normalized emission spectra of PS-N-PMA-A sample in three selected solvents differing in the methanol content (excited at 275 nm) are shown in Fig. 3. Individual spectra were normalized by the maximum naphthalene emission close to 335 nm. A comparison of anthracene emission bands in the region 380–450 nm shows an increasing NRET effect with increasing CH_3OH content. Slightly different levels of the baseline at low emission wavelengths, λ, close to the excitation, are caused by the light scattering that is weak in molecular and strong in micellar solutions. In a mixture with 5 vol.% CH_3OH, the polymer dissolves in the form of individual polymer coils. The anthracene-tagged end of PMA block is on average far from the block junction where naphthalene is attached. The energy transfer is therefore weak and the emission (curve *1*) is mainly caused by direct excitation of anthracene at 275 nm. A mixture containing 67 vol.% CH_3OH is a fairly strong selective precipitant for PS and micelles with segregated PS cores and PMA shells occur in the solution. The anthracene emission increases with respect to that of naphthalene (curve *2*). It indicates that the anthracene-tagged ends of shell-forming PMA blocks recoil slightly back towards the core. If the ends of PMA blocks were significantly stretched and oriented towards the bulk solvent, similarly to PMA conformations in regu-

lar PS-PMA micelles, the NRET effect would be negligible since the average donor-to-trap distance would reach *ca* 50–60 nm (based on DLS measurements). Curve *3* shows the emission spectrum in a mixture with 85 vol.% CH_3OH. The sensitized anthracene emission is only a little stronger than that in the previous case. In this paper, we do not evaluate the NRET efficiency from the sensitized anthracene emission. In our previous paper, we have shown that this is in principle possible (in combination with the directly excited spectra of anthracene), provided that all appropriate corrections had carefully been done[58]. Nevertheless, the corrections are quite tricky and we have shown that this evaluation is less reliable than that based on naphthalene emission. The inset shows the integrated naphthalene and anthracene emission intensities as functions of the solvent composition. Curve *1′* shows the naphthalene (*i.e.*, donor) intensity, I_D^0, in the absence of traps, measured for PS-N-PMA sample (excitation at 275 nm), curve *2′* the NRET-quenched naphthalene emission in PS-N-PMA-A sample. Both curves almost overlap up to 40 vol.% of CH_3OH. In micellar systems, we observe the fluorescence quenching by energy transfer to anthracene. The sensitized anthracene emission (which contains *ca* 50% contribution of

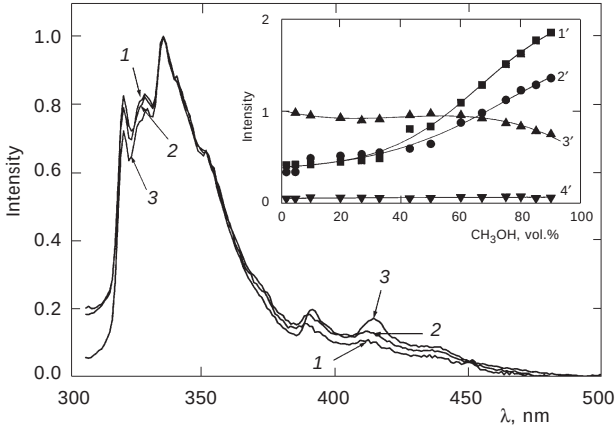

FIG. 3

The normalized emission spectra of the PS-N-PMA-A sample (excitation at 275 nm) in 1,4-dioxane–methanol mixtures with 5 (*1*), 67 (*2*) and 85 vol.% CH_3OH (*3*), relative intensities normalized by the maximum emission at 335 nm. Inset: Fluorescence emission intensities as functions of the solvent composition: naphthalene tag in PS-N-PMA sample (*1′*) and in PS-N-PMA-A sample (*2′*), directly excited anthracene emission (at 370 nm) from PS-N-PMA-A (*3′*) and the NRET-sensitized anthracene emission (excited at 275 nm) from PS-N-PMA-A (*4′*), fluorescence intensities in arbitrary units (measured with constant widths of excitation and emission slits)

the direct excitation) does not almost depend on the solvent composition (curve *4'*). However, the directly excited anthracene emission (excited at 370 nm) reveals the static quenching in polar methanol-rich mixtures (curve *3'*). The ratio (I_T^{sens}/I_T^{dir}) increases and (I_D^q/I_D^0) decreases with increasing content of CH_3OH (not shown), which indicates the increasing NRET effect. For the evaluation of the excitation energy transfer efficiency, χ_{tr}, we have used only naphthalene emissions, because this evaluation is more reliable than that based on the sensitized anthracene emission[58].

Time-Resolved Fluorescence Measurements

Since the transfer efficiency, χ_{tr}, may be obtained from time-resolved fluorescence measurements with a high accuracy and reliability (much better than that from steady-state measurements), we have measured also the time-resolved naphthalene fluorescence decays in both micellar systems. The transfer efficiency χ_{tr} was evaluated from the well-known formula[60]

$$\chi_{tr} = 1 - \frac{\left\langle \tau_D^q \right\rangle}{\left\langle \tau_D^0 \right\rangle}, \qquad (6)$$

where $\langle \tau_D^q \rangle$ and $\langle \tau_D^0 \rangle$ are the mean fluorescence lifetimes of the donor in the presence and absence of energy traps, respectively. The mean fluorescence lifetime (the linear one, which is appropriate for evaluation of quantum yields and NRET from time-resolved measurements) is defined by the relation $\langle \tau_D \rangle = \Sigma_i A_i \tau_i$, where A_i and τ_i are the normalized pre-exponential factors and lifetime components in the time-resolved fluorescence decays, $I_D(t)$, respectively.

Typical time-resolved fluorescence data from micelles in a mixture with 80 vol.% CH_3OH are depicted in Fig. 4. Curve *1* shows the non-quenched naphthalene fluorescence decay from PS-N-PMA (unaffected by NRET) and curve *2* the quenched decay from PS-N-PMA-A micelles. The decays are not single-exponential; however, both curves almost superimpose at early times. The NRET quenching effect is fairly weak and becomes evident only at medium and longer times. This suggests that the early non-exponential decay in both curves (*i.e.*, the initial quenching) is mainly caused by chemical attachment of the fluorophore to the polymer chain and possibly also by impurities in copolymer samples. The mean fluorescence lifetimes for both systems are shown in the inset as functions of the solvent composition. Non-exponential decays are quite common in polymer systems with

chemically attached fluorophores[15,27] since (i) tagging of the chain is random, (ii) chain conformations in the vicinity of the fluorophore fluctuate and (iii) fluorescence is very sensitive to impurities indicating their presence even if their content is extremely low. As a result, only few fluorophores show perfect single-exponential decays after attachment to polymer chain (*e.g.*, phenanthrene)[61].

The energy transfer efficiency, χ_{tr}, based on the steady-state fluorescence intensities of the quenched and non-quenched donor (*i.e.*, naphthalene excited at 275 nm, collected in the 310–450 nm region) using Eq. (*5*) is represented by curve *1* in Fig. 5 and that based on the time-resolved measurements is depicted by curve *2*. A comparison of both curves is interesting. It is generally recognized that time-resolved measurements yield accurate and reliable data while steady-state measurement may be negatively influenced by a number of complicating factors. The comparison shows that the properly corrected steady-state measurement provides fairly reasonable data. However, it is necessary to keep in mind that the corrections and all auxiliary measurements have to be performed very carefully. They may change the raw data by a factor of 2–3 and that are very sensitive not only to micellar mass and size, but also to refractive index and other optical properties of the solvent. Therefore, we do not recommend quantitative study of micellar systems using the steady-state NRET measurement only.

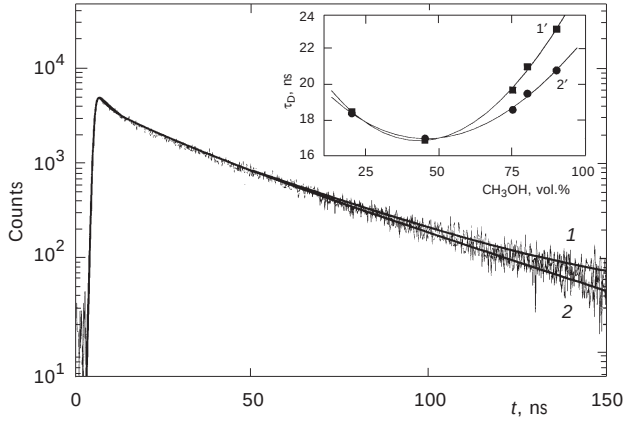

FIG. 4

Time-resolved fluorescence decays from the tagged polymeric samples in 1,4-dioxane–methanol (80 vol.%): naphthalene tag in PS-N-PMA (*1*) and in PS-N-PMA-A (*2*). Inset: The mean fluorescence lifetimes, $\langle\tau_F\rangle$, as functions of the solvent composition: naphthalene tag in PS-N-PMA (*1′*) and in PS-N-PMA-A (*2′*)

The NRET effect is generally weak (especially when compared with that in 1,4-dioxane–water mixtures)[58]; however, it is well-measurable in CH_3OH-rich mixtures with 1,4-dioxane. The difference is easy understandable since methanol is an organic solvent and is much less polar than water. Nevertheless, the strongly nonpolar anthracene shows a fairly strong tendency to hide in the micellar shell.

Numerical Results of Model Monte Carlo Computer Simulations

We model polymeric micelles according to experimental characteristics of polystyrene-*block*-poly(methacrylic acid) micelles, double-tagged with naphthalene (between blocks) and with anthracene (at the end of the poly(methacrylic acid) block) in highly polar solvents. Using experimental values, $M_w = 10.6 \cdot 10^6$ g mol^{-1} for a 1,4-dioxane–CH_3OH (80 vol.%) mixture, together with molecular characteristics of unimers, we get the association number, n_{as} *ca* 175 and the radius of the core, R_C *ca* 12.5 nm (assuming density of polystyrene *ca* 1.0 g cm^{-3})[62]. This R_C value is very close to that which we have recently obtained for a very similar micellizing system in water by small angle neutron scattering[63]. In simulations, we use $n = 200$ for simplicity. Methanol is a significantly milder precipitant for PS than water; however, we have found in our earlier studies of PS-PMA micelles that the PS cores are also compact in methanol-rich mixtures and the

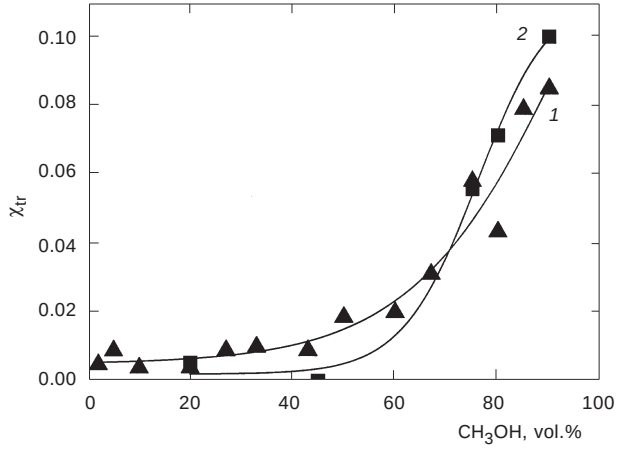

FIG. 5

The nonradiative excitation energy transfer efficiency, χ_{tr}, as a function of the solvent composition: evaluated from the steady-state naphthalene emission (*1*) and from the naphthalene fluorescence decays (*2*). The curves are just guidelines for eyes

association numbers are similar to those in aqueous buffers[15,27]. For the Förster radius, we use, R_0 = 2.1 nm which was reported in literature for the naphthalene-to-anthracene energy transfer in a nonpolar medium[64].

The donor fluorescence decays, $I_D^q(t)/I_D^0(t)$, and the excitation energy transfer efficiency, χ_{tr} (inset), calculated for 3D-random model are shown in Fig. 6. The transfer efficiency is represented as a function of R_H (and also as a function of the average distance of traps, $\langle r \rangle$ from the core center) and the fluorescence decays are depicted as functions of the reduced time, t/τ_D, for a few selected R_H values. The donor fluorescence decays are strongly non-exponential since the configurations of traps fluctuate among individual micelles. The closest donor-trap distance is small in some micelles, but it can be long in others. The energy transfer is therefore important in a certain fraction of micelles, while the remaining fraction of micelles behaves as a system unaffected by NRET. It is evident that the NRET efficiency and non-exponential shapes of $I_D^q(t)/I_D(t)$ curves depend strongly on R_H. As far as the 3D model is concerned, the experimental value of the energy transfer efficiency, χ_{tr} *ca* 0.1, requires a low value of the hydrodynamic radius of micelles, R_H = 26 nm, which is in sharp contrast to the experimental value of R_H *ca* 80 nm. Therefore, we do not consider the 3D model as a realistic physical model that might reasonably describe the distribution of pendant hydrophobic traps in the shell of PS-PMA micelles in polar solvents.

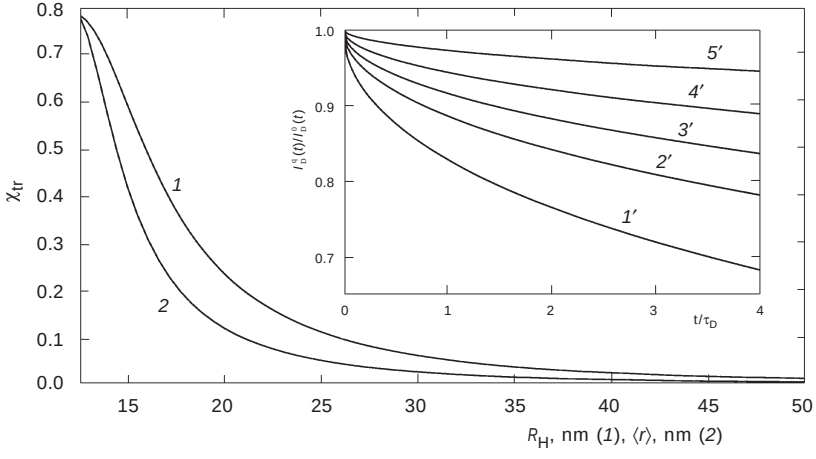

FIG. 6

The nonradiative excitation energy transfer efficiency, χ_{tr}, as a function of the hydrodynamic radius of micelles, R_H, for the 3D-random model with R_C = 12.5 nm and the Förster radius, R_0 = 2.1 nm. Inset: The time-resolved donor emissions $I_D^q(t)/I_D^0(t)$ for R_H = 22.6 (*1′*), 25.6 (*2′*), 28.2 (*3′*), 32.0 (*4′*) and 40.2 nm (*5′*)

The results of simulations for 2D-random model and for the simplistic reference model are shown in Figs 7 and 8, respectively. The mutually corresponding curves based on both models are very similar for medium and

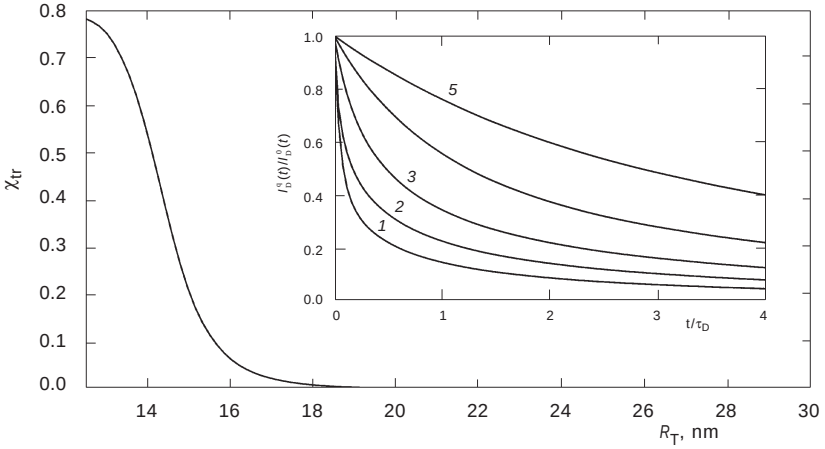

FIG. 7

The nonradiative excitation energy transfer efficiency, χ_{tr}, as a function of the distance of traps from the core/shell interface, R_T, for the 2D-random model with R_C = 12.5 nm and the Förster radius, R_0 = 2.1 nm. Inset: The time-resolved donor emissions $I_D^q(t)/I_D^0(t)$ for R_T = 12.5 (*1*), 13.5 (*2*), 14.0 (*3*), 14.5 (*4*) and 15.0 nm (*5*)

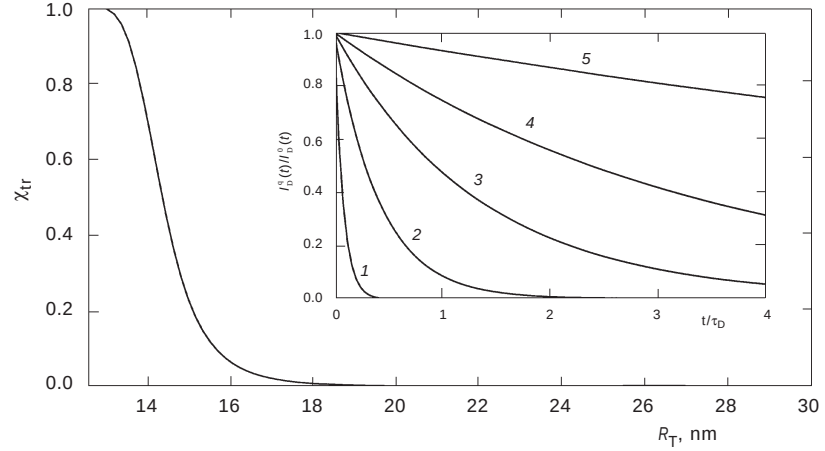

FIG. 8

The nonradiative excitation energy transfer efficiency, χ_{tr}, as a function of the distance of traps from the core/shell interface, R_T, for the simplistic reference model with R_C = 12.5 nm and the Förster radius, R_0 = 2.1 nm. Inset: The time-resolved donor emissions $I_D^q(t)/I_D^0(t)$ for R_T = 13.5 (*1*), 14.0 (*2*), 14.5 (*3*), 15.0 (*4*) and 16.0 nm (*5*)

large R_T (R_T larger than 15 nm which corresponds roughly to the $2R_0$ distance of traps from the core/shell interface). The curves based on the simplistic "uniform" model are always single-exponential – according to the theory. The non-exponential deviations for curves based on the 2D model are also negligible for $R_T > 15$ nm.

Results of simulations for the Maxwellian model are shown in Fig. 9 for several values of $\langle r \rangle = R_C + 2\sigma\sqrt{(2/\pi)}$, *i.e.*, for different average distances of traps from the core center. They are generally non-exponential. As compared with curves for 3D model, the non-exponential nature of curves based on the M model, *i.e.*, the difference between ratios $(\mathrm{d}f(t)/\mathrm{d}t)/f(t)$ for short and long times, t, where $f(t) = I_D^q(t)/I_D(t)$, is slightly more pronounced for $\chi_{tr} \geq 0.3$, and less pronounced for smaller χ_{tr} (which is well apparent, *e.g.*, for χ_{tr} *ca* 0.1).

For comparison of simulated and experimental data, it is necessary to keep in mind that the experimental fluorescence decay from the non-quenched naphthalene in PS-N-PMA micelles is not single-exponential. Nevertheless, the ratio of the quenched and non-quenched decays may be reasonably compared with the results of Monte Carlo simulations. The comparison of the fitted experimental decay, $I_D^q(t)/I_D(t)$, *vs* $t/\langle\tau\rangle$, with corresponding simulated decays is shown in Fig. 10, for the energy transfer efficiency, $\chi_{tr} = 0.1$ (*i.e.*, for PS-N-PMA-A micelles in a mixture with 90 vol.%

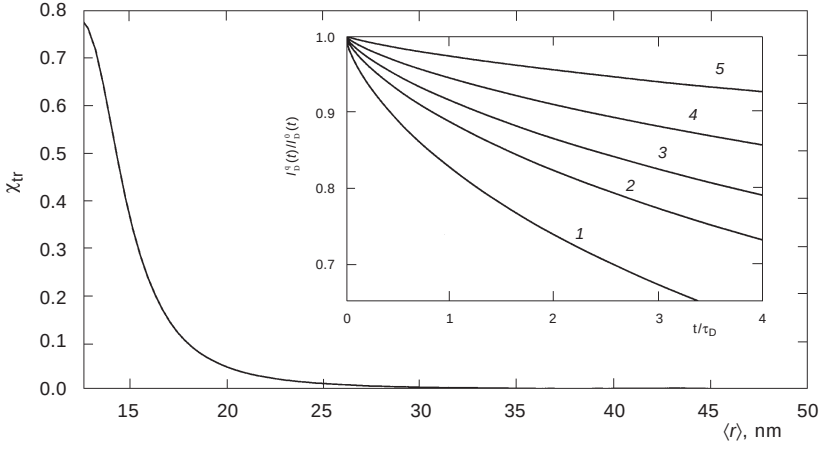

FIG. 9

The nonradiative excitation energy transfer efficiency, χ_{tr}, as a function of $\langle r \rangle = R_C + 2\sigma\sqrt{(2/\pi)}$ for the fully random angular and the Maxwellian radial distribution of traps in the shell with $R_C = 12.5$ nm and the Förster radius, $R_0 = 2.1$ nm. Inset: The time-resolved donor emissions $I_D^q(t)/I_D^0(t)$ for $\chi_{tr} = 0.15$ (*1*), 0.10 (*2*), 0.075 (*3*), 0.05 (*4*) and 0.025 nm (*5*)

CH_3OH). It is evident that the experimental curve (curve *1*) compares best with that based on the Maxwellian model (curve *4*). Nevertheless, it is necessary to keep in mind that differences between individual curves, even though well discernible, are not large for low values of the energy transfer efficiency. However, it is evident without any doubts that traps are buried relatively deep in the shell in methanol-rich solvents. The average distances of traps from the core center, evaluated according to any of the model used, are fairly small. The simplistic model yields R_T *ca* 16 nm, while the M model yields the corresponding value $\langle r \rangle$ = 18 nm in the 1,4-dioxane–methanol (90 vol.%) mixture. This means that the average distance of traps from the core shell/interface is *ca* 5 nm in micelles with the hydrodynamic radius of *ca* 75 nm. In contrast to the aqueous systems studied earlier[58], it seems that the distribution of traps in the shell of micelles in 1,4-dioxane–methanol solvents is fairly uniform. A comparison of time-resolved decays favors the non-symmetrical Maxwell-type distribution function with a tail, but the experimental curve does not show any sign that the real spatial distribution of traps may be a function with two peaks (which was the case of modified micelles in aqueous mixtures[58]).

Numerical results, obtained by Monte Carlo simulations for the above described models show that simultaneous measurement of the donor steady-state spectra and time-resolved donor fluorescence decays are necessary in studies of the distribution of traps in micellar shells in double-tagged poly-

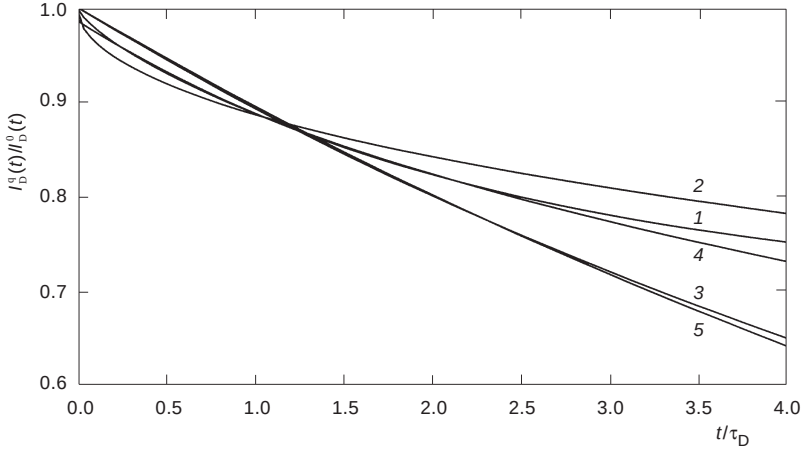

FIG. 10

The fitted experimental naphthalene fluorescence decay, $I_D^q(t)/I_D^0(t)$ *vs* t/τ_D for the energy transfer efficiency χ_{tr} = 0.1 (*1*), compared with several corresponding simulated curves for the 3D model (*2*), 2D model (*3*), Maxwellian model (*4*) and simplistic reference model (*5*)

meric micelles. Realistic and fairly detailed models are needed for the analysis of fluorescence data[65]. The model has to be based on the body of knowledge obtained by a number of different experimental techniques and general thermodynamic considerations. The proposed structure of the shell of (i) non-modified (right hand part of the cartoon) and (ii) hydrophobically modified PS-PMA micelles (left hand part) in non-aqueous polar solvents is presented in Scheme 1.

CONCLUSIONS

1. Computer-based study of nonradiative excitation energy transfer in dilute solutions of hydrophobically modified, double-tagged amphiphilic block copolymer micelles in polar solvents allows us to analyze and interpret results of experimental measurements. The nonpolar energy traps that are attached at the ends of the shell-forming blocks try to avoid contact with solvent molecules. Since the shell-forming blocks are significantly less polar than the solvent, the traps bury themselves in the shell and pull the ends of the shell-forming blocks back towards the core, forcing the chains either to collapse or to form loops. A distribution of traps in the shell is the result of the competition between the enthalpy gain and the entropy loss associated with formation of collapsed conformations or loops. The results of simulations provide a basis for interpretation of experimental fluorescence data.

2. The results of the study show that the time-resolved measurements (not the steady-state measurements alone) allow for the determination of the type of the distribution function of traps in the shell. The simulated curves are necessary for fitting experimental data in order to obtain structural characteristics of real micellar systems.

3. The results of light scattering and fluorescence measurements confirm that the nonpolar anthracene tags at the ends of PMA blocks try to avoid the polar solvent and return back into the shell. As compared with similar hydrophobically modified micellar systems in aqueous media[58], the nonradiative excitation energy transfer from naphthalene to anthracene is weaker, which is in agreement with a lower tendency of anthracene to avoid the methanol-rich medium than that of the aqueous medium.

4. The NRET from naphthalene to anthracene quenches slightly the naphthalene emission in micellar systems. A comparison of experimental decay curves with those simulated suggests that in methanol-rich solvents, the anthracene traps penetrate relatively deep in the inner shell. The average distance of anthracene traps from the core is larger that that in water,

but the difference makes only a few nanometers. The experimental decays compare best with those based on the Maxwellian model. The comparison shows clearly that the models assuming a broad distribution of traps (*e.g.*, 3D-random model) are not able to reproduce satisfactorily the time-resolved fluorescence data for the experimental structural characteristics of micelles.

The Czech authors would like to acknowledge financial support by the Grant Agency of the Czech Republic (Grant No. 203/01/0536) and by the Grant Agency of the Charles University (Grant No. 215/2000/BCh/PřF). S. E. Webber would like to acknowledge the support from the Robert A. Welch Foundation (Grant F-356). The computer simulations were performed using the computer facilities of the Computer-Meta-Center (Praha–Brno–Plzeň) of the Ministry of Education, Youth and Sports of the Czech Republic.

REFERENCES

1. Winnik M. A. in: *Photophysical and Photochemical Tools in Polymer Science* (M. A. Winnik, Ed.), NATO ASI Series C, Vol. 182. Reidel, Dordrecht 1986.
2. Demchenko A. P. in: *Topics in Fluorescence Spectroscopy* (J. R. Lakowics, Ed.), Vol. 3. Plenum Press, New York 1991.
3. Morawetz H.: *Science* **1988**, *240*, 172.
4. Nakashima K., Winnik M. A., Dai K. H., Kramer E. J., Washiyama J.: *Macromolecules* **1992**, *25*, 6866.
5. Ni S., Zhank P., Wang Y., Winnik M. A.: *Macromolecules* **1994**, *27*, 5742.
6. Rhabi Y., Yekta A., Winnik M. A., DeVoe R. J., Barrera D.: *Macromolecules* **1999**, *32*, 3241.
7. Holden D. A., Guillet J. E.: *Macromolecules* **1980**, *13*, 289.
8. Liu G., Guillet J. E., Al-Takrity T. B., Jenkins A. D., Walton D. R. M.: *Macromolecules* **1991**, *24*, 68.
9. Major D. M., Torkelson J. M., Brearley A. M.: *Macromolecules* **1990**, *23*, 1700.
10. Ringsdorf H., Simon J., Winnik F. M.: *Macromolecules* **1992**, *25*, 7306.
11. Yekta A., Duhamel J., Brochard P., Adiwidjaja H., Winnik M. A.: *Macromolecules* **1993**, *26*, 1829.
12. Farinha J. P. S., Schillén K., Winnik M. A.: *J. Phys. Chem. B* **1999**, *103*, 2487.
13. Liu G., Smith C. K., Hu N., Tao J.: *Macromolecules* **1996**, *29*, 220.
14. Tuzar Z., Kratochvíl P. in: *Surface and Colloid Science* (E. Matievic, Ed.), Vol. 15, p. 1. Plenum Press, New York 1993.
15. Procházka K., Kiserow D., Ramireddy C., Tuzar Z., Munk P., Webber S. E.: *Macromolecules* **1992**, *25*, 449.
16. Wilhelm M., Zhao C.-L., Wang Y., Xu R., Winnik M. A., Mura J.-L., Riess G., Croucher M. D.: *Macromolecules* **1991**, *24*, 1033.
17. Mössmer S., Spatz J. P., Möller M., Aberle T., Schmidt J., Burchardt W.: *Macromolecules* **2000**, *33*, 4791.
18. Astafieva I., Zhong X. F., Eisenberg A.: *Macromolecules* **1993**, *26*, 7339.
19. Astafieva I., Khougaz K., Eisenberg A.: *Macromolecules* **1995**, *28*, 7127.
20. Yu Y. S., Zhang L. F., Eisenberg A.: *Langmuir* **1997**, *13*, 2578.

21. Zhang L. F., Eisenberg A.: *Macromolecules* **1999**, *32*, 2239.
22. Shen H. W., Eisenberg A.: *J. Phys. Chem. B* **1999**, *103*, 9473.
23. Shen W. H., Eisenberg A.: *Macromolecules* **2000**, *33*, 2561.
24. Antonietti M., Heinz S., Schmidt M., Rosenauer C.: *Macromolecules* **1994**, *27*, 3276.
25. Regenbrecht M., Akari S., Förster S., Mohwald H.: *J. Phys. Chem. B* **1999**, *103*, 6669.
26. Lee A. S., Gast A. P., Buthun V., Armes S. P.: *Macromolecules* **1999**, *32*, 4302.
27. a) Kiserow D., Procházka K., Ramireddy C., Tuzar Z., Munk P., Webber S. E.: *Macromolecules* **1992**, *25*, 454; b) Kiserow D., Procházka K., Ramireddy C., Tuzar Z., Munk P., Webber S. E.: *Macromolecules* **1992**, *25*, 461.
28. Tian M., Quin A., Ramireddy C., Webber S. E., Munk P., Tuzar Z., Procházka K.: *Langmuir* **1993**, *9*, 1741.
29. Teng Y., Morrison M., Munk P., Webber S. E., Procházka K.: *Macromolecules* **1998**, *31*, 3578.
30. a) Štěpánek M., Krijtová K., Limpouchová Z., Procházka K., Teng Y., Webber S. E., Munk P.: *Acta Polym.* **1998**, *49*, 96; b) Štěpánek M., Krijtová K., Limpouchová Z., Procházka K., Teng Y., Webber S. E., Munk P.: *Acta Polym.* **1998**, *49*, 103.
31. Procházka K., Martin T. J., Munk P., Webber S. E.: *Macromolecules* **1996**, *29*, 6518.
32. Štěpánek M., Procházka K.: *Langmuir* **1999**, *15*, 8800.
33. Štěpánek M., Procházka K., Brown W.: *Langmuir* **2000**, *16*, 2502.
34. Procházka K.: *J. Phys. Chem.* **1995**, *99*, 14108.
35. Viduna D., Limpouchová Z., Procházka K.: *Macromolecules* **1997**, *30*, 7263.
36. Limpouchová Z., Viduna D., Procházka K.: *Macromolecules* **1997**, *30*, 8027.
37. Jelínek K., Limpouchová Z., Procházka K.: *Macromol. Theory Simulations* **2000**, *9*, 703.
38. Tuzar Z., Kratochvíl P.: *Collect. Czech. Chem. Commun.* **1967**, *32*, 3358.
39. Jakeš J.: *Czech. J. Phys. B* **1988**, *38*, 1305.
40. van der Meer W. B., Coker G., Chen S. S.-Y.: *Resonance Energy Transfer*. Wiley-VCH, New York 1991.
41. Förster T.: *Discuss. Faraday Soc.* **1959**, *7*, 27.
42. Yang C. L., Evesque P., El-Sayed M. A.: *J. Phys. Chem.* **1985**, *89*, 3442.
43. Klafter J., Blumen A.: *J. Lumin.* **1985**, *34*, 77.
44. Blumen A., Klafter J., Zumhofen G.: *J. Chem. Phys.* **1986**, *84*, 1397.
45. Gochanour C. R., Andersen H. C., Fayer M. D.: *J. Chem. Phys.* **1979**, *70*, 4254.
46. Ediger M. D., Fayer M. D.: *J. Chem. Phys.* **1983**, *78*, 2518.
47. Baumann J., Fayer M. D.: *J. Chem. Phys.* **1986**, *85*, 4087.
48. Ediger M. D., Dominique R. P., Fayer M. D.: *J. Chem. Phys.* **1988**, *89*, 5224.
49. Farinha J. P. S., Martinho J. M. G., Yekta A., Winnik M. A.: *Macromolecules* **1995**, *28*, 6084.
50. Farinha J. P. S., Martinho J. M. G., Kawagushi S., Yekta A., Winnik M. A.: *J. Phys. Chem.* **1996**, *100*, 12552.
51. Yekta A., Winnik M. A., Farinha J. P. S., Martinho J. M. G.: *J. Phys. Chem. B* **1997**, *101*, 1787.
52. Shusharina N. P., Linse P.: *Eur. Phys. J. E* **2001**, *4*, 399.
53. Wijmans C. M., Zhulina E. B.: *Macromolecules* **1993**, *25*, 7214.
54. Zhulina E. B., Birshtein T. M., Borisov O. V.: *Macromolecules* **1995**, *28*, 1491.
55. Israels R., Leermakers F. A. M., Fleer G. J.: *Macromolecules* **1994**, *27*, 3087.
56. Lyatskaya Yu. V., Leermakers F. A. M., Fleer G. J., Zhulina E. B., Birsthein T. M.: *Macromolecules* **1995**, *28*, 3562.

57. Uhlík F., Limpouchová Z., Matějíček P., Procházka K., Tuzar Z., Webber S. E.: *Macromolecules*, submitted.
58. Matějíček P., Uhlík F., Limpouchová Z., Procházka K., Tuzar Z., Webber S. E.: *Macromolecules*, submitted.
59. Martin T. J., Webber S. E.: *Macromolecules* **1995**, *28*, 8845.
60. Lakowicz J. R.: *Principles of Fluorescence Spectroscopy*. Plenum Press, New York 1983.
61. Rhabi Y., Winnik M. A.: *Macromolecules* **2001**, *34*, 5238.
62. Brandrup J., Immergut E. H. (Eds): *Polymer Handbook*. Interscience Publishers, New York 1967.
63. Pleštil J., Kříž J., Tuzar Z., Procházka K., Melnichenko Yu. B., Wignall G. D., Talingting M. R., Munk P., Webber S. E.: *Macromol. Chem. Phys.* **2001**, *202*, 553.
64. Berleman I. B.: *Energy Transfer Parameters of Aromatic Compounds*. Academic Press, New York 1973.
65. Uhlík F., Limpouchová Z., Procházka K.: Unpublished results.